Bio-Inspired Fuzzy Logic–Based Passive Vision Coordination for UAVs

Gonzalo Garcia[1] and Azim Eskandarian[2]

Abstract— **This paper presents a bio-inspired swarm coordination framework for unmanned aerial systems that extends prior passive-vision-based approaches by replacing crisp pixel-based proximity comparisons with a decentralized fuzzy logic inference mechanism. Previous works achieved swarm cohesion by directly comparing apparent sizes of neighboring agents across opposing visual sectors, using pixel measurements as indirect distance cues; however, this relied on hard thresholds and binary decisions that can induce discontinuous velocity corrections. In the proposed framework, relative visual proximity cues are instead processed through a fuzzy logic system that more closely reflects biological perception. The fuzzy formulation enables smooth, graded velocity corrections based on relative closeness assessments across lateral and newly introduced vertical visual sectors, improving stability and reducing oscillatory behavior. Each agent operates autonomously using only passive monocular vision, without explicit distance estimation, inter-agent communication, or centralized coordination. Simulation results show smoother trajectories, reduced control effort, and improved positional coherence compared to the crisp strategy, while preserving robustness to sensing uncertainty and scalability. Preliminary flight tests further validate the approach and support fuzzy perception-driven control as a biologically consistent alternative for vision-based swarm coordination on resource-constrained aerial platforms.**

I. INTRODUCTION

Coordinated motion of multiple unmanned aerial vehicles (UAVs) is of growing interest for applications such as environmental monitoring, search and rescue, infrastructure inspection, and operation in GNSS-denied environments. Swarm-based approaches are particularly attractive due to their scalability, robustness, and reliance on decentralized control inspired by biological collective behavior [1], [2]. Vision-based swarm coordination has emerged as a promising solution, as cameras are lightweight, passive, and energy-efficient while providing rich perceptual information. Compared to active sensors, vision enables covert operation and is well suited for resource-constrained platforms [3], [4]. Works in [5], [6] showed learning vision-Based flights with guaranteeing results. However, achieving reliable coordination using only visual information, without range estimation or communication, remains challenging. In prior work [7], the authors proposed a passive-vision strategy in which UAVs inferred relative proximity from apparent feature sizes in monocular imagery. By balancing measurements across opposing image sectors, agents maintained spacing and achieved stable swarm behavior. However, the use of crisp thresholds can lead to abrupt control actions and sensitivity to noise. Biological systems instead rely on qualitative perception and graded responses under uncertainty [8]–[10]. Fuzzy logic provides a natural framework for such reasoning, enabling smooth control through linguistic rules without requiring precise models [11]–[13]. Motivated by this, the present work introduces a decentralized fuzzy-logic extension to the passive vision framework. Apparent feature sizes are mapped to linguistic variables and evaluated through a compact rule base to generate smooth velocity corrections. The method also extends visual sectorization vertically to improve 3D coordination. Simulation and flight results show improved smoothness, reduced oscillations, and enhanced coherence, while preserving the scalability and robustness of the original approach. The remainder of the paper is organized as follows. Section 2 reviews the passive-vision swarm logic, Section 3 presents the fuzzy-logic reformulation, Section 4 discusses simulation and experimental results, and Section 5 concludes the paper.

[1]Gonzalo Garcia is with the College of Engineering, Virginia Commonwealth University, 601 West Main St. Richmond, VA 23284, USA garciaga3@vcu.edu

[2]Azim Eskandarian is with the Faculty of the College of Engineering, Virginia Commonwealth University, 601 West Main St. Richmond, VA 23284, USA eskandariana@vcu.edu

II. PERCEPTION-DRIVEN SWARMING LOGIC BASED ON PASSIVE VISION

A. Bio-Inspired Visual Sectorization Geometry

Early experimental studies, such as [8], revealed that interactions within bird flocks exhibit non-uniform angular structures in three dimensions. Subsequent work by [9] showed that collective flocking behavior is governed by topological rather than metric interactions, with each bird responding to a limited set of nearest neighbors regardless of global density. These findings support interaction models based on qualitative, locally perceived cues rather than explicit distance measurements.

The swarming framework adopted in this work follows this biologically inspired principle by avoiding explicit metric distance estimation. Instead, agents regulate their motion using relative perceptual information derived from local passive vision. This assumption is particularly relevant for interior agents, whose sensing may be partially occluded and who lack global awareness or leadership roles. Qualitative assessments of perceived proximity therefore provide a plausible and robust mechanism for maintaining cohesion.

Accordingly, each agent partitions its surrounding space into a set of visual sectors defined relative to its instantaneous position, direction of motion, and body-fixed reference frame, as illustrated in Figure 1. Building on earlier implementations with two vertical divisions [7], [14], the present formulation introduces three vertical layers (upper, central, and lower), allowing finer discrimination of relative spatial relationships in three dimensions. Combined with lateral segmentation, this yields eighteen lateral sectors distributed around the agent, along with six forward-looking sectors spanning the same vertical layers. A rear blind region is retained, consistent with biological visual constraints.

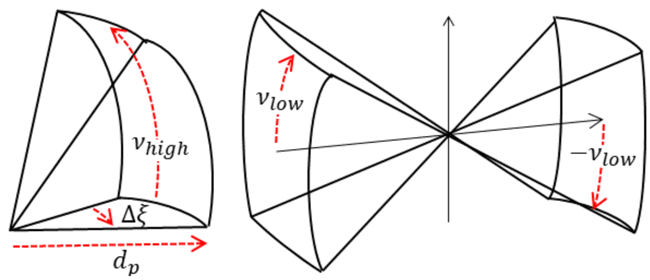

Fig. 1. Sector creation for opposed sectors is based in [7]. Three vertical divisions have been included in this work. **Left**: Original upper lateral sector, showing the vertical angle ν_{high}, lateral angle $\Delta\xi$, and radius d_p. **Right**: Creation of new sector covering the center, defined by angle ν_{low}.

All sectors are defined within a maximum perception radius d_p, interpreted as a preferred interaction distance, while their angular extents are specified by lateral angle $\Delta\xi$ and vertical angles ν_{high} and ν_{low}. The number of sectors, angular resolution, and sensing radius are tunable parameters selected to match vehicle dynamics and sensing limitations.

This refined sectorization preserves the decentralized and biologically plausible nature of the approach while enabling relative comparisons across both lateral and vertical directions. Such structure is essential for achieving stable three-dimensional swarm motion using passive vision alone.

B. Relative Proximity Evaluation and Motion Regulation

The proposed swarming logic operates without explicit measurement of inter-agent distances. Instead, each agent continuously evaluates relative proximity relationships among neighboring agents detected within its visual sectors. This process is inspired by biological perception, where decisions are based on comparative assessments, such as nearer versus farther, rather than exact numerical quantities. At each update step, an agent processes onboard visual data through the following steps: **1) Neighbor selection**: For each agent j and sector, the closest visible neighbor is identified using apparent size cues. **2) Opposed-sector comparison**: Relative proximity is evaluated between opposing sector pairs (e.g., left–right, upper–lower, and diagonal combinations). **3) Forward regulation**: Neighbors in forward sectors are compared to a desired proximity p_d^f, selected based on expected motion direction. **4) Incomplete perception**: If a sector lacks a neighbor, it is assigned a preferred proximity reflecting equilibrium spacing. **5) Motion regulation**: Each comparison yields a corrective velocity component $\Delta\boldsymbol{v}_i^j$ from the perspective of agent i that drives perceptual balance.

Unlike crisp, binary logic that classifies neighbors as simply "closer" or "farther," this framework is intentionally formulated in terms of relative perceptual differences, allowing graded motion responses. The resulting velocity corrections are vectorially combined, $\Delta\boldsymbol{v}^j = \sum_i \Delta\boldsymbol{v}_i{}^j$, and added to the nominal agent's velocity to generate smooth, decentralized motion updates.

$$\boldsymbol{V}^j \leftarrow \boldsymbol{V}^j + \Delta\boldsymbol{v}^j \tag{1}$$

This formulation establishes a natural bridge to fuzzy reasoning: relative proximity is evaluated qualitatively across sectors, and corrective actions are applied proportionally rather than as fixed-magnitude impulses. The explicit fuzzy inference mechanism used to implement this reasoning is introduced later as a separate system-level component.

C. Apparent-Size–Based Depth Cues

Depth perception in biological collectives often relies on indirect visual cues rather than explicit range estimation. In bird flocks, limited binocular overlap and depth-of-field suggest that relative distance is inferred from apparent size, motion, and occlusion instead of precise stereoscopic measurements [15]. Inspired by these observations, the proposed approach estimates relative proximity using apparent-size cues extracted from monocular images. Assuming that all agents are physically similar, variations in perceived size provide a reliable qualitative indicator of relative distance: larger apparent size implies closer proximity, while smaller size indicates greater separation. Rather than converting this information into precise metric range, apparent size is used directly as a relative depth cue. By comparing apparent sizes across opposing visual sectors, each agent assesses its relative position within the local neighborhood and applies corrective motion to reduce perceptual imbalance, driving the swarm toward cohesion through purely local interactions.

In the current implementation, apparent-size cues are extracted through simple logical processing of binary visual detections. Two onboard LEDs with fixed relative placement on the Crazyflie 2+ micro-UAV [16] serve as visual markers during flight tests; however, other salient features, such as shape, color, or texture, could also be used. Tracking this marker pair enables reliable estimation of relative inter-agent proximity from monocular imagery without inter-agent communication or unique identifiers. The measured pixel-based separation, sep_{meas}, provides a compact representation of relative proximity. When a metric estimate is required, sep_{meas} is mapped to physical distance using a precomputed calibration lookup table, f_e [7]

$$dist_{raw} = f_e(sep_{meas}) \tag{2}$$

which relates apparent marker separation in pixels to the corresponding inter-drone distance.

Each image frame is binarized by thresholding pixel intensities using an empirically selected value $0 < t_r < int_{max}$. Connected components are extracted and filtered by area, and among the remaining candidates, the pair with the smallest centroid separation and approximate horizontal alignment is selected as the marker pair $\{m_l, m_r\}$. Marker identities are maintained across frames via nearest-neighbor centroid association, allowing continuous tracking and automatic recovery from temporary detection failures at low computational cost.

Figure 2 illustrates a 324×244 pixels grayscale image, with detected markers and the corresponding thresholded binary image, demonstrating the simplicity and robustness of the apparent-size–based depth cue extraction process.

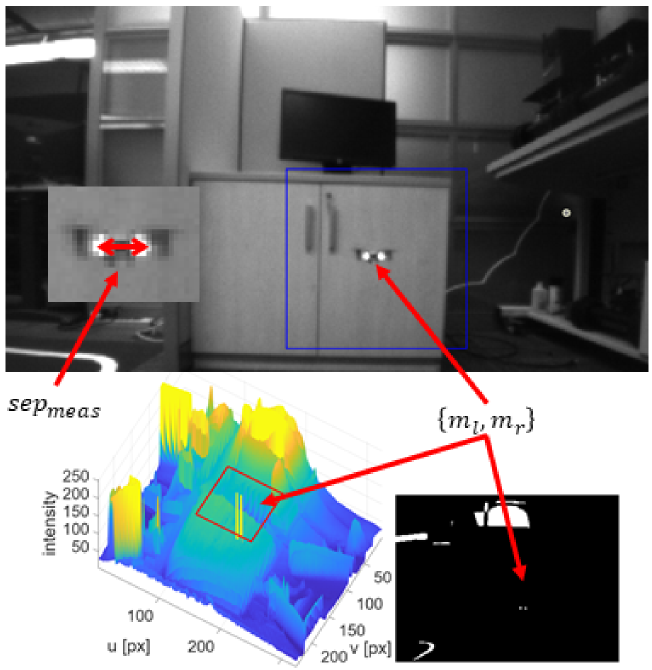

Fig. 2. Image processing. **Top**: Grey-color image showing tracking of retained markers $\{m_l, m_r\}$ (inset: inter-distance $dist_{raw}$ using Eq. 2 and pixel separation sep_{meas} . **Bottom**: Three-dimensional visualization of pixel intensities, and binary image after thresholding, $t_r = 230$.

III. FUZZY LOGIC–BASED RELATIVE PROXIMITY REGULATION

A. Fuzzy Representation of Relative Visual Proximity

The perception-driven swarming framework described previously relies on qualitative assessments of relative proximity derived from monocular visual information. To formalize this process and enable smooth, robust motion regulation, the present work replaces crisp comparisons of apparent size with a fuzzy logic–based representation of relative proximity.

For each visual sector, the apparent size of the closest detected neighbor is mapped to linguistic variables describing relative proximity, such as near, average, and far. Measurements are fuzzified using overlapping membership functions, allowing partial membership across categories. This representation eliminates discontinuities caused by hard thresholds and improves robustness to visual noise, occlusions, and transient detection errors by producing smooth velocity corrections.

The same fuzzification process is applied consistently across all lateral and forward sectors, and across all vertical layers introduced in the refined sectorization scheme. This uniform treatment ensures that the control logic remains decentralized, scalable, and independent of global references. The fuzzification process is illustrated in Figure 3 (Top), which shows the overlapping membership functions (left and right) used to map the apparent visual size into the linguitic proximity categories near, average, and far.

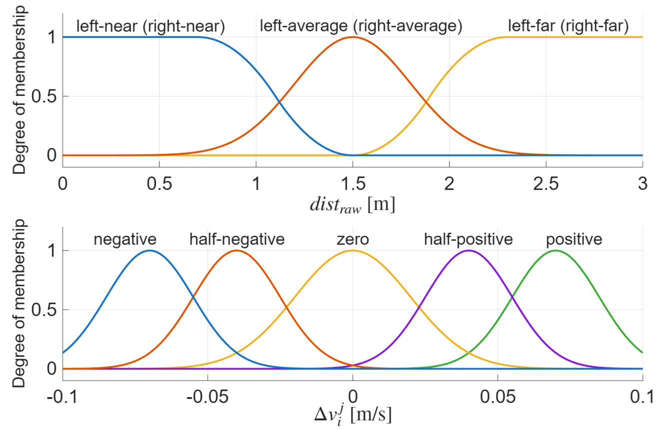

Fig. 3. Membership functions. **Top**: Input membership functions for opposed sectors (left and right) as a function of distance $dist_{raw}$. **Bottom**: Output membership functions for Δv_i^j (see Eq. 1)

B. Sector-Based Fuzzy Inference for Velocity Correction

Motion regulation is achieved by applying a sector-wise fuzzy inference process that compares the relative proximity of neighbors detected in opposed sector pairs. For each pair of sectors (e.g., left–right, upper–lower, or diagonally opposed sectors across vertical layers), a fuzzy rule base determines the corrective velocity contribution along the corresponding axis. The inference mechanism follows a symmetric and biologically intuitive structure. For a representative opposed sector pair, the fuzzy rule set is defined as in Table I:

TABLE I
BIO-INSPIRED FUZZY RULE STE

If	Then
left is near and right is near	Δv is zero
left is near and right is average	Δv is half-positive
left is near and right is far	Δv is positive
left is average and right is near	Δv is half-negative
left is average and right is average	Δv is zero
left is average and right is far	Δv is half-positive
left is far and right is near	Δv is negative
left is far and right is average	Δv is half-negative
left is far and right is far	Δv is zero

This 9-rule structure enforces perceptual balance: corrective motion arises only from asymmetries between opposed sectors, with magnitude reflecting the degree of imbalance. The same inference is applied independently across all sector pairs, including vertical and forward directions, each producing a signed velocity contribution Δv_i^j. These contributions are summed to yield the final corrective velocity, preserving decentralization and allowing multiple weak cues to jointly influence motion, consistent with biological swarm behavior. The fuzzy velocity outputs and membership functions are shown in Figure 3 (Bottom), illustrating how perceptual asymmetries map to smooth corrective commands.

Compared to direct size comparison, the method achieves smoother convergence, improved stability, and increased robustness to sensing uncertainty while maintaining minimal sensing and communication requirements.

C. Comparative Stability and Cohesion Analysis Under Steady-State Conditions

To evaluate stability and qualitative benefits, the proposed fuzzy-logic coordination strategy was compared with the previous crisp pixel-based sector balancing approach. The analysis aimed to verify preservation of convergence and cohesion while assessing whether fuzzy inference produces smoother, less aggressive transients. For each method, 100 simulations were conducted with three agents initialized at randomized positions and orientations. Agents relied solely on passive monocular vision, without distance estimation, communication, or centralized control. All pairwise inter-agent distances were recorded, yielding 300 trajectories per method as a measure of cohesion and convergence.

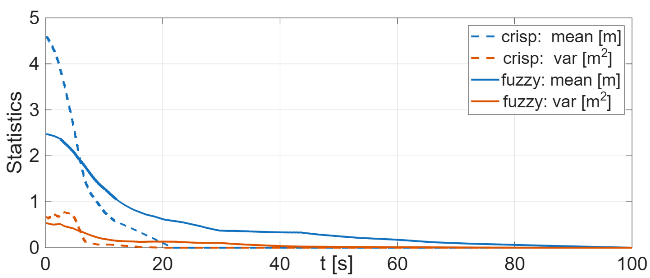

Fig. 4. Comparative steady-state cohesion analysis of crisp sector balancing and the proposed fuzzy strategy. Mean and variance of pairwise inter-agent distances are shown 100 simulations with random initial conditions. Both methods converge to stable formations, while the fuzzy approach exhibits smoother transients and reduced variance, indicating lower corrective effort.

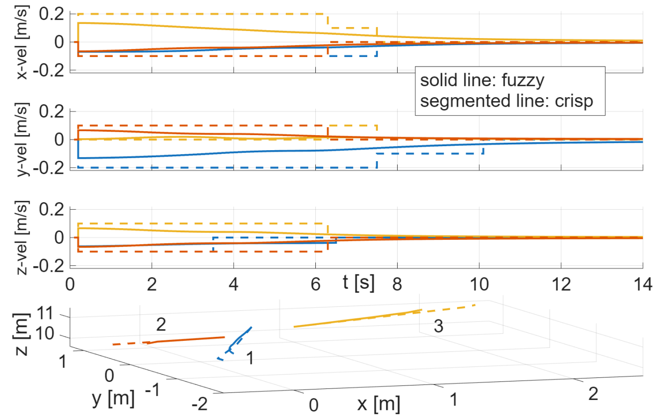

Fig. 5. Comparison between the previous crisp coordination method (segmented lines) and the proposed fuzzy-logic-based strategy (solid lines). **Top**: Velocity components of the three agents (blue: 1, red: 2, orange: 3) under both methods, illustrating differences in transient responses and convergence behavior. **Bottom**: Corresponding 3D trajectories of the agents for both approaches, showing the overall motion patterns and resulting inter-agent spacing.

Figure 4 presents the sample mean and variance of inter-agent distances over time for both the crisp approach [7] and the proposed fuzzy strategy. In both cases, the mean distance converges to a stable steady-state value despite significant variability in initial conditions, confirming that the fuzzy reformulation preserves the stability properties of the original pixel-based logic. Notable differences arise during the transient phase. The fuzzy-based approach exhibits a more gradual decrease in the mean and variance of inter-agent distances, indicating smoother convergence, whereas the crisp strategy produces larger fluctuations due to hard decision thresholds. The reduced variance under the fuzzy formulation reflects fewer and smaller corrective motions enabled by graded velocity responses.

Figure 5 illustrates representative results from a single simulation run under identical initial conditions, showing velocity components and corresponding 3D trajectories for both methods. The comparison highlights smoother velocity profiles and less oscillatory behavior for the fuzzy strategy, while both methods converge to cohesive formations.

Overall, this analysis confirms that while both approaches achieve stable swarm cohesion, the proposed fuzzy logic–based coordination yields smoother convergence, reduced oscillations, and lower corrective effort. Similar stability tests with larger number of agents conducted in [7], [14], [17] complement these results. This was further confirmed by separately simulating 15 agents, with both approaches showing convergence to steady state values, and with final interdistances sample distributions approaching crisp: $N(5.8, 5.9)$ and fuzzy: $N(3.7, 1.4)$. These properties are particularly advantageous for real-world UAV deployments, where excessive motion can amplify sensing noise, energy consumption, and control coupling effects. The results support fuzzy inference as a biologically consistent and practically superior enhancement to crisp pixel-based sector balancing for vision-based swarm coordination.

IV. TESTING RESULTS

Simulations and flight experiments were conducted to validate the proposed fuzzy logic–based passive vision coordination strategy under realistic sensing and control conditions. The geometry of the bio-inspired sector was configured using lateral angles $\{\xi_1 = 30°, \xi_2 = 70°, \xi_3 = 110°, \xi_4 = 150°\}$ [7], a preferred distance between agents $d_p = 3$ m, and a preferred forward distance $d_p^f = 1.3\, d_p$. Vertical detection was defined by angles $\nu_{high} = 80°$ and $\nu_{low} = 30°$. The maximum corrective speed applied by the coordination logic was limited to $|\Delta v_i| = 0.1$ m/s, while the nominal swarm velocity was set to $|V| = 0$. For the inner loop, the Crazyflie firmware employs a cascaded low-level control architecture consisting of position, velocity, attitude, and angular-rate control loops to actuate the rotors [16].

A. Simulated Flights

The simulations were carried in Simulink using the Crazyflie dynamics [17], including its low-level flight controller, and involved three vehicles and both the previous and proposed coordination strategies. Figure 6 (Top) shows attitude angles of drone 1 (blue: commanded; red: measured) for both approaches, while the yaw angle was regulated to zero. The oscillations observed could be reduced through further tuning of the low-level controller gains.

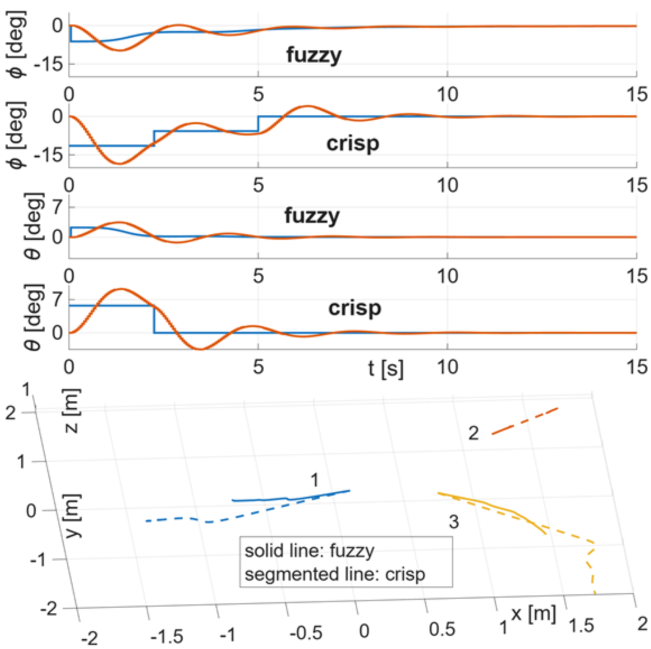

Fig. 6. **Top**: Equivalent roll and pitch command angles derived from the corresponding velocity commands. **Bottom**: 3D trajectories, both showing improved performance with the proposed fuzzy approach.

B. Flight Test Configurations

Three independent flight tests were performed using two Crazyflie 2+ drones, one acting as a visual reference in hovering, and the other actively regulating its relative position using only onboard monocular vision. No inter-agent communication or explicit range sensing was employed. During each flight test, the follower UAV adjusted its horizontal motion to maintain the desired visual separation, remain laterally centered within the image plane, and maintain a constant altitude relative to the hovering reference drone. In the proposed framework, the swarm coordination logic generates commanded horizontal velocities $(v_{x_{cmd}}, v_{y_{cmd}})$, which are passed directly to the onboard velocity/attitude controller, based on the following errors

$$\begin{aligned} \text{longitudinal:} \quad & e_{dist} = dist_{cmd} - dist_{filtered} \\ \text{lateral:} \quad & e_{lat} = u_{cmd} - u_{filtered} \end{aligned} \tag{3}$$

The filtered quantity $u_{filtered}$ corresponds to the horizontal image-plane coordinate of the geometric center of the two detected markers, while $dist_{filtered}$ is obtained from the marker separation following the steps described previously. Both raw measurements, $dist_{raw}$ and u_{raw}, are smoothed using a low-pass filter to produce the filtered signals $dist_{filtered}$ and $u_{filtered}$. These quantities are then converted into commanded longitudinal and lateral velocities, as follows

$$\begin{aligned} \text{longitudinal:} \quad & v_{x_{cmd}} = k_e^{v_x} \cdot e_{dist} \\ \text{lateral:} \quad & v_{y_{cmd}} = k_e^{v_y} \cdot e_{lat} \end{aligned} \tag{4}$$

with $k_e^{v_x}$ and $k_e^{v_y}$ proportional gains to be tuned experimentally. For this test $dist_{cmd} = 10[px]$, and $u_{cmd} = 324/2 = 162[px]$ corresponding to the component of the center of the camera. These velocities were fed into the inner controllers.

These commands, which are saturated at a maximum magnitude of $5[cm/s]$, are then tracked by the lower-level attitude and rate controllers to produce the required motion. This structure allows the bio-inspired coordination and fuzzy logic modules to operate independently of the inner-loop stabilization dynamics, leveraging the existing flight controller for reliable execution. Additional details on the Crazyflie control architecture can be found in [16].

C. Visual Tracking Robustness

For each test, Figure 7 reports the number of visual markers detected over time $num_{markers}$, illustrating the robustness of the perception pipeline. While the optimal case corresponds to detecting both onboard LEDs, temporary occlusions, illumination changes, or motion blur may reduce the number of detected markers to one or zero, or increase them beyond 2. Despite these intermittent mistakes, the algorithm reacquired the markers without requiring reinitialization. Importantly, even when the number of detected markers varies, the estimated pixel separation sep_{meas} remains smooth and well behaved, demonstrating that the logical processing and temporal association mechanisms effectively filter transient detection failures and maintain stable proximity estimation throughout the maneuver.

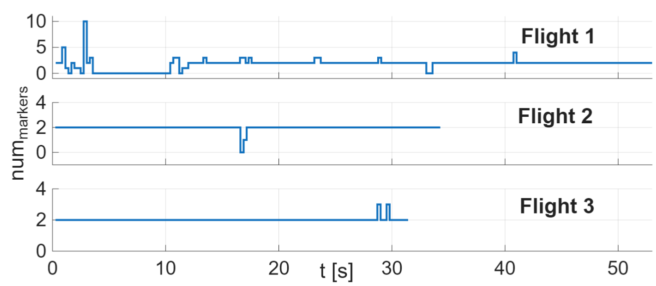

Fig. 7. Number of visual markers detected over time during flight tests. Although the optimal case corresponds to detecting both onboard LEDs ($num_{markers} = 2$), temporary losses due to occlusions, illumination changes, or motion blur occur. Despite these variations, the estimated pixel separation sep_{meas} remains smooth, demonstrating robust marker reacquisition and stable proximity estimation.

D. Visual Distance and Lateral Position Estimation

Figure 8 presents, for each flight test, the estimated inter-agent distance $dist_{raw}$, obtained from pixel separation using the calibration mapping in Eq. 2, along with the lateral image-plane position u_{raw} of the tracked markers' centroid. These quantities are shown together with their filtered counterparts, $dist_{filtered}$ and $u_{filtered}$, and the corresponding commanded references, $dist_{cmd}$ and u_{cmd}.

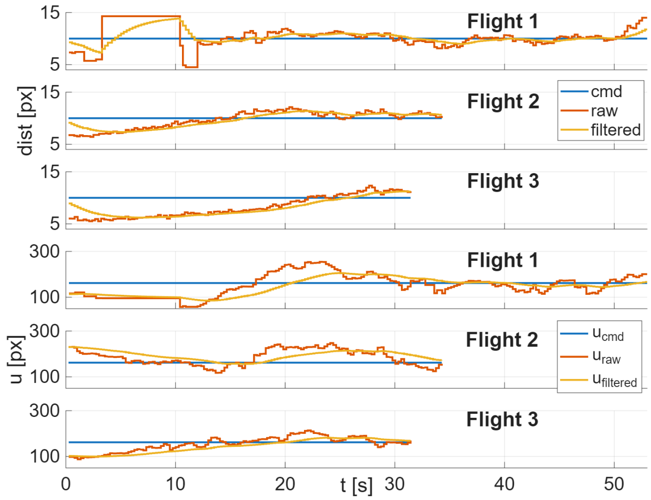

Fig. 8. Estimated inter-agent distance $dist_{filtered}$ and lateral image-plane position $u_{filtered}$ during flight tests, shown together with their commanded references $dist_{cmd}$ and u_{cmd}. Distance is obtained from the pixel separation via the calibration mapping in Eq. 2. Both quantities converge smoothly toward their desired values.

In all three flight tests, both signals converged smoothly toward their desired values. The distance estimate exhibits limited noise and no observable drift, confirming the reliability of apparent-size-based depth cues in a real flight environment. Similarly, the lateral position error remains bounded and centered, indicating that the follower UAV maintains visual alignment with the reference drone.

E. Velocity Commands and Closed-Loop Response

Figure 9 shows for each flight test, the commanded longitudinal and lateral velocities, $\{v_{x_{cmd}}, v_{y_{cmd}}\}$, computed from the visual tracking errors according to Eqs. 3, 4. These velocity commands are fed directly into the Crazyflie's inner control loops to generate horizontal motion.

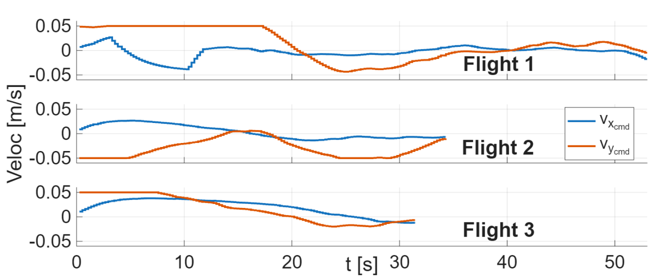

Fig. 9. Commanded longitudinal and lateral velocities $\{v_{x_{cmd}}, v_{y_{cmd}}\}$ generated during flight tests, from visual tracking errors using Eqs. 3–4. The velocity profiles are smooth and bounded, saturated at a maximum of $0.05[m/s]$ illustrating gradual corrective motion and stable closed-loop behavior under the proposed fuzzy logic coordination strategy.

The velocity profiles across all tests are smooth and bounded, with no abrupt transitions, reflecting the graded nature of the fuzzy inference mechanism. Corrective motions are applied gradually as visual imbalance is detected and reduced as equilibrium is approached. This behavior contrasts with the sharper velocity changes typically induced by crisp, threshold-based logic and demonstrates the benefit of fuzzy reasoning for real-world implementation. Overall, the flight tests consistently show that the proposed fuzzy logic passive-vision framework enables stable relative positioning, smooth control action, and robust operation despite intermittent visual detection losses.

V. CONCLUSIONS

This paper proposed a bio-inspired, vision-based swarm coordination framework that replaces crisp proximity comparisons with decentralized fuzzy logic inference. Using only passive monocular vision, UAVs infer relative proximity from apparent-size cues within a sectorized perception space, enabling smooth velocity corrections without distance estimation, communication, or centralized control. Compared to the crisp sector-balancing approach, simulations and flight tests with micro-UAVs demonstrate smoother convergence, reduced corrective effort, and stable behavior under sensing uncertainty, validating practical feasibility on lightweight platforms with limited sensing and computation. These results show that fuzzy logic enables biologically inspired, perception-driven coordination in real flight without explicit distance sensing or inter-agent communication, providing a practical enhancement for resource-constrained aerial swarms.

REFERENCES

[1] E. Sahin. Swarm robotics: From sources of inspiration to domains of application. In *Swarm Robotics*, volume 3342 of *Lecture Notes in Computer Science*, pages 10–20. Springer, 2005.
[2] M. Brambilla, E. Ferrante, M. Birattari, and M. Dorigo. Swarm robotics: A review from the swarm engineering perspective. *Swarm Intelligence*, 7(1):1–41, 2013.
[3] F. Caballero, L. Merino, J. Ferruz, and A. Ollero. Vision-based odometry and slam for medium and high altitude flying uavs. *Journal of Intelligent and Robotic Systems*, 54:137–161, 2009.
[4] N. Michael, J. Fink, and V. Kumar. Cooperative manipulation and transportation with aerial robots. *Autonomous Robots*, 30(1):73–86, 2011.
[5] F. Schilling, J. Lecoeur, F. Schiano, and D. Floreano. Learning vision-based flight in drone swarms by imitation. *IEEE Robotics and Automation Letters*, 4(4):4523–4530, October 2019.
[6] F. Schilling, F. Schiano, and D. Floreano. Vision-based drone flocking in outdoor environments. *IEEE Robotics and Automation Letters*, 6(2):2954–2961, April 2021.
[7] G. Garcia and A Eskandarian. Bio-inspired uas swarm-keeping based on computer vision. In *ICUAS*, pages 99–105, 2025.
[8] P. F. Major and L. M. Dill. The three-dimensional structure of airborne bird flocks. *Behavioral Ecology and Sociobiology*, 4:111–122, 1978.
[9] M. Ballerini et al. Interaction ruling animal collective behavior depends on topological rather than metric distance: evidence from a field study. *Proc. Natl. Acad. Sci. U.S.A.*, 105:1232–1237, 2008.
[10] C. Reynolds. Flocks, herds, and schools: a distributed behavioral model. *Computer Graphics*, 21(4):25–34, 1987.
[11] L. A. Zadeh. Fuzzy sets. *Inf. and Control*, 8(3):338–353, 1965.
[12] E. H. Mamdani. Application of fuzzy algorithms for control of a simple dynamic plant. *Proc. of the IEE*, 121(12):1585–1588, 1974.
[13] Kevin M. Passino and Stephen Yurkovich. *Fuzzy Control*. Addison-Wesley, 1998.
[14] G. A. Garcia and S. S. Keshmiri. Biologically inspired trajectory generation for swarming uavs using topological distances. *Aerospace Science and Technology*, 54:312–319, 2016.
[15] G. R. Martin. What is binocular vision for? a birds' eye view. *Journal of Vision*, 9(11):1–19, 2009. Article 14.
[16] Crazyflie 2.1+. https://www.bitcraze.io/products/crazyflie-2-1-plus/.
[17] G. Garcia, A. R. Kim, E. Jackson, S. Keshmiri, and D. Shukla. Modeling and flight control of a commercial nano quadrotor. In *ICUAS 2017*, Miami, FL, USA, June 2017. IEEE.